Chemical Science

Accepted Manuscript

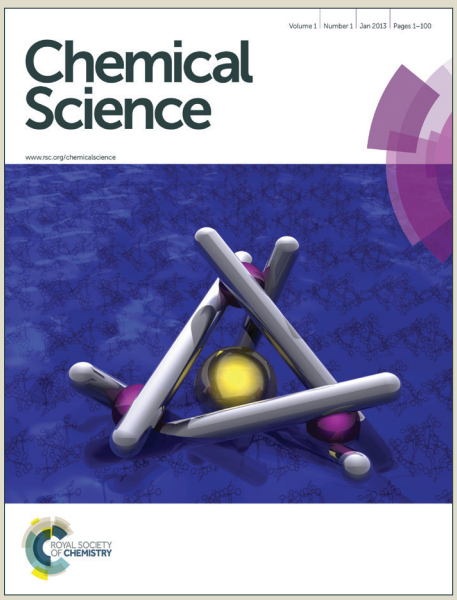

ROYAL SOCIETY OF CHEMISTRY

www.rsc.org/chemicalscience

Chemical Science

RSCPublishing

EDGE ARTICLE

The Edge Termination Controlled Kinetics in Graphene Chemical Vapor Deposition Growth

Cite this: DOI: 10.1039/x0xx00000x

Haibo Shu,[ab] Xiaoshuang Chen[b] and Feng Ding[*ab]

Received ooth January 2014,
Accepted ooth January 2014

DOI: 10.1039/x0xx00000x

www.rsc.org/

Understanding the kinetics of graphene chemical vapor deposition (CVD) growth is crucial for desired graphene growth. Depending on the partial pressure of hydrogen in carrier gas, temperature and the type of substrate, both armchair (AC) and zigzag (ZZ) edges of graphene can be either passivated by metal surface or terminated by hydrogen atoms. Owing to the large barrier for incorporating C atoms, the growth rate of H terminated graphene edges is significantly slower than that of metal surface passivated ones. Based on this understanding, various behaviours and the kinetics of graphene growth at different temperatures, H_2 pressure and on various catalyst surfaces are satisfactorily explained and the strategy of growing edge-controlled graphene domains is predicated.

1. Introduction

Graphene has attracted great attention since 2004[1] due to its exceptional physical properties, such as extremely high carrier mobility, excellent thermal conductivity and extraordinary mechanical strength, etc. These properties ensure graphene a great potential for a large number of applications, such as high performance field effect transistors (FETs), energy generation and storage, sensors, composite materials, metal free catalysts, etc. To realize these applications, especially those in high performance electronics, it is critical to synthesize the large-area graphene with controlled crystallinity, edge type, and the number of layers. Among numerous methods of grapheme synthesis, the transition metal catalyzed chemical vapour deposition (CVD) method is broadly recognized as the most promising approach to achieve this target. Various transition metals, such as Au, Cu, Ni, Co, Pd, Pt, Rh, Ir, Ru and their alloys, have been used as the catalysts for the CVD growth. To facilitate the experimental design for preferred graphene growth, many theoretical approaches have been carried recently[2-14] but the understanding of graphene growth at atomic level is still very limited.

Recently, more and more experimental evidences suggest that the shape, quality, and the number of layers of the CVD-grown graphene strongly depend on the H_2 content in the gas flow. For example, graphene domains grown on Cu surface present versatile shapes. Under low H_2 pressure or high CH_4:H_2 ratio, the graphene domains normally present the fractal-like branched shape[15-18]. In contract, with high H_2 flow, most graphene domains present a regular hexagonal shape with zigzag edges[19-24]. The graphene domains grown on Au surface are known to have similar behaviour as those formed on Cu surface.[10] Differently, graphene domains grown on the active catalyst such as Ni, Co, Pt, Ru, Rh, surfaces are mostly in a regular hexagonal shape.[25-30]

It is known that the fractal-liked graphene shape must be understood based on the diffusion limited growth in which the edge of crystal is highly active for atom/molecule adsorption and the feedstock supply near the edge is limited.[31] In contrast, a regular graphene edge can be explained based on the orientation dependent growth rates by applying the well-known theory of kinetic Wulff construction (KWC)[32] that the fast growing edges will quickly disappear.

To understand the versatile experimental observations during grapheme CVD growth, we systematically explored the termination of graphene edges on various catalyst surfaces (Au, Cu, Ni, Co) and the incorporation process of carbon onto these edges. Our results demonstrate two modes of graphene CVD growth: If a graphene edge is passivated by metal surface (**M-G**), the addition of C atoms is fast because of the high activity of the edge. On the other hand, if a graphene edge is terminated by H atoms (**H-G**), the addition of C atoms is slow because of the edge inertness. Moreover, our study has revealed a mechanism for controlling the edge structure of graphene domains by adjusting the growth parameters.

2. Computational Details

In this study, density-functional theory (DFT) total-energy calculations were performed by using the Vienna *ab initio* Simulation Package (VASP)[33,34]. The exchange-correlation energy was described in the generalized-gradient approximation (GGA) using the PBE functional[35]. Considering the concerned energies in this study are mainly attributed by the chemical binding between graphene edge and the catalyst surface, the GGA method should be sufficient. The energy cutoff for the plane-wave expansion was set to 400 eV, using the projector augmented wave (PAW) potentials[36] to describe the electron-ion interaction. The geometry optimization was performed by using the conjugate gradient scheme until the force acting on each atom is less than 0.01 eV/Å.

To investigate the structural stability of graphene edges on transitional metal (TM) surfaces (Au, Cu, Ni, and Co), a four-layer metal slab with the fixed bottom layer atoms was used to represent the metal surfaces, then the pristine and H-terminated graphene nanoribbons (GNRs) were put on the metal surfaces (see Fig. 1 and Fig. S1 in the ESI†), respectively. The repeated slabs were separated by ~ 12 Å to eliminate their interactions, and the allowed lattice mismatch of GNR-metal interfaces in the constructed slab models was smaller than 3%. The unit cells of surface slab are 4.43 Å × 15.34 Å and 17.71 Å × 2.56 Å for the AC and ZZ graphene edges on Cu(111) surface, respectively. Similar models were used to investigate the stability of GNRs on Au, Ni, and Co surfaces. The

unit cells of AC-GNRs on Au, Ni, and Co surfaces are 8.65 Å ×14.98 Å, 4.32 Å × 14.95 Å, and 4.34 Å × 17.55 Å, respectively. For the ZZ-GNRs on Au, Ni, and Co surfaces, their unit cells are 23.07 Å × 4.99 Å, 21.58 Å × 2.49 Å, and 26.05 Å × 2.51 Å, respectively. The corresponding *k*-point meshes are 6×2×1 for metal-supported AC edges and 2×6×1 for metal-supported ZZ edges, respectively. The above settings were obtained on the basis of a series of tests for the energy convergence with respect to the k-point mesh setting and the thickness of vacuum layer (see ESI, Fig. S2† and Fig. S3†) and the calculated results showed that the settings used in the present calculations can supply enough accuracy.

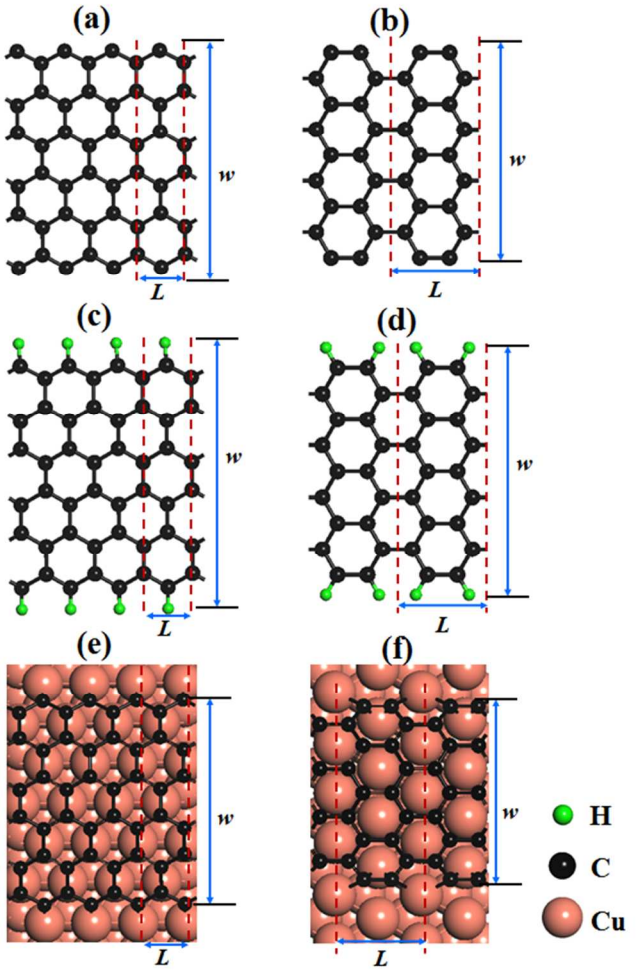

Fig. 1 Freestanding, H terminated and transition metal surface (Cu(111)) passivated graphene AC (a, c, e) and ZZ (b, d, f) edges. *w* and *L* denote the width of GNRs and the length of unit cell along the periodic direction, respectively.

The stability of graphene edges was evaluated by calculating their formation energies. For the freestanding graphene edges, their formation energies E_f are defined as,

$$E_f = [2E(w) - E(2w)]/2L, \quad (1)$$

where *w* and *L* is the ribbon width and the length of unit cell along the periodic direction, $E(w)$ and $E(2w)$ are the energies of GNRs with the width of *w* and 2*w*. Here the used width *w* of AC and ZZ GNRs is 9.84 Å and 11.36 Å respectively and the length *L* of unit cell along AC and ZZ directions are 4.26 Å and 2.46 Å, respectively. The formation energies of H-passivated graphene edges were calculated by

$$E_f = E_f(G) + [E(H) - E(G) - n_H E_H]/2L, \quad (2)$$

where $E(H)$, $E(G)$ and E_H are the energies of H-passivated GNR, freestanding GNR, and H atom in hydrogen molecule, respectively. $E_f(G)$ is the formation energies of freestanding GNR. n_H is the number of H atoms in the H-passivated GNR. For the metal-supported GNR, their formation energies are were calculated by

$$E_f = [2E_T(w) - E_T(2w) - E_M]/2L, \quad (3)$$

where $E_T(w)$ and $E_T(2w)$ are the energies of metal-supported GNRs with the width of *w* and 2*w* respectively, and E_M is the total energy of metal substrate. The models for calculating the formation energies of metal-supported GNRs are shown in Fig. S4†. Such a computational model can eliminate the effect of van der Waals interaction between GNR and metal substrate on the formation energies of graphene edges.

ab initio molecular dynamics (MD) simulations were carried out to investigate the role of graphene edges in the incorporation of carbon atoms on Cu(111) surface. In the calculations, we used the models with the surface slabs of 8.85 Å × 15.34 Å for the growth of AC-edges and 17.71 Å × 7.67 Å for the growth of ZZ-edges. Considering the huge timing consumption of running MD simulation for a large system (there are 120 and 123 atoms in the models of AC and ZZ edges), Gamma-only *k*-point was used in the calculations for the Brillouin-zone integration.[7,37] MD simulations were performed in the canonical (NVT) at 1500 K with a 1.0 fs time step.

3. Results and Discussion

Firstly, let's consider the structural stability of various graphene edges. An unpassivated graphene edge (Fig. 1a and Fig. 1b) possesses very high formation energies due to the formation of dangling bonds at the edge and therefore is very unstable. As listed in Table 1, the formation energies are as high as 10.01 and 11.84 eV/nm for the armchair (AC) and zigzag (ZZ) graphene edges, respectively. In contrast, the hydrogenation of unpassivated edges (Fig. 1c and Fig. 1d) leads to a notably reduction of the formation energies and a notable enhancement of the stability. It can be found that their formation energies are only 0.20 and 0.90 eV/nm for AC and ZZ edges, respectively. If a freestanding graphene edge is placed on a metal surface (Fig. 1e and Fig. 1f), the edge will be bent to the metal surface and be passiavted spontaneously.[10,38] On the Co(0001) or Ni(111) surfaces, the graphene edge is more stable than that on Cu(111) or Au(111) surface due to their high activity on the metal surfaces.

Table 1 Formation energies of armchair (AC) and zigzag (ZZ) graphene edges (in eV/nm) in vacuum, terminated by H atoms and on metal surfaces. Here the energy of H_2 molecule is used as reference. The atomic structures of these graphene edges are shown in Fig. 1.

	None	H	Au	Cu	Co	Ni
AC	10.01	0.20	8.73	7.38	5.26	5.38
ZZ	11.84	0.90	7.84	5.52	3.98	3.61

From above discussion, we can conclude that, during the graphene CVD growth, an unpassivated edge is not stable and it should be either passivated by the metal surface (**M-G**) or be terminated by the H atoms (**H-G**).[39] Next let's turn the competition between the two types of edges under the condition of CVD growth. Considering the high temperature of graphene CVD growth, the free-energy difference between a **H-G** and a **M-G** edge can be written as:

$$\Delta G = \Delta E_f + \Delta F_{vib} - N_H \times \mu_H(T, P), \quad (4)$$

where ΔE_f is the difference of formation energy between the H-G and the M-G edges, ΔF_{vib} is the vibrational free energy of H atoms at the H-G edge, N_H is the number of H atoms, and μ_H is the chemical potential of the H_2 gas as a function of H_2 partial pressure *p* and temperature *T* (see the details in the ESI†).

Fig. 2 shows the thermodynamic diagrams of graphene AC and ZZ edges on Au, Cu, Co and Ni surfaces as the functions of *T* and *p*. It can be found that the termination type of graphene edges in CVD growth highly depends on the *T*, *p* and the type of metal substrates.

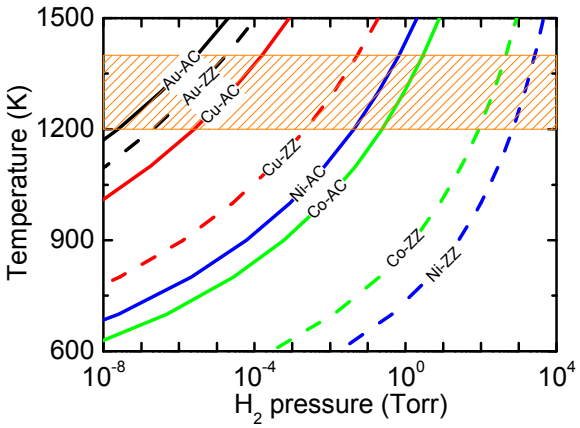

Fig. 2 The diagrams of AC and ZZ graphene edges on Au, Cu, Co, Ni surfaces as the functions of temperature and H_2 partial pressure, respectively. The patterned area denotes the typical experimental temperature range of graphene CVD growth.

On the widely used metal substrate, Cu(111) surface, the phase transition from the H-G to the M-G requires H_2 pressure of ~ 10^{-2} Torr for the ZZ edge and H_2 pressure of ~10^{-5} Torr for the AC edge in the temperature range of 1200 ~ 1400 K (typical CVD growth temperature, see Table S1 of ESI†), respectively. Such a result reveals that graphene edges are mostly passivated by metal surface in the low-pressure CVD growth (LPCVD)[12,40] and H-terminated graphene edges may occur in the atmospheric pressure CVD growth (APCVD) on Cu surface[13, 40-42]. When H_2 pressure lies between 10^{-2} and 10^{-5} Torr, ZZ edge tends to be passivated by metal surface and AC edge tends to be H-terminated. Hence, the diagram can be divided into three regions: (***i***) the M-G edges dominating the growth at high *T* and low *p*; (***ii***) the H-G edge dominating the growth at low *T* and high *p* and (***iii***) the AC edges are terminated by H but the ZZ edges are passivated by the metal surface at medium *T* and *p*.

On Au, Ni, Co surfaces, similar characteristics as those for Cu are presented but the transition from the **H-G** to the **M-G** occurs at very different (*T, P*). In the range of typical graphene CVD growth temperature (1200~1400 K), the edge phase transition from the **H-G** to the **M-G** on Au(111) surface requires the H_2 pressure below ~10^{-6} to 10^{-7} Torr, which is nearly impossible unless the pressure of H_2 is very carefully controlled. This implies that, during graphene CVD growth on Au surface at a typical growth condition, the graphene edges should be terminated by H atoms. On Ni(111) and Co(0001) surfaces, the H_2 pressure of edge phase transition increases to ~ 0.1 Torr for the AC edge and ~ 100 Torr for the ZZ edge, respectively. In view of experimental growth conditions (see Table S1†), the H_2 pressure is generally kept in the range of 10^{-4} ~ 10^{2} Torr and the growth temperature is mostly maintained at ~1300 K. Therefore, the graphene growth on Ni(111) and Co(0001) surfaces are mostly dominated by the **M-G** edges.

It is worthy to mention that the C solubility in Ni and Co at the temperature of graphene CVD growth is high.[43,44] The diffusion of C atoms into the metal substrates may lead to the formation of surface carbide. In order to understand how the carbide affects the graphene edge-metal surface interaction, the formation energies of graphene edges on Ni(111) and Co(0001) with surface carbide have been calculated (see the details in the ESI†). We find that the formation energies of armchair/zigzag graphene edge on the Ni_2C and Co_2C surface carbides are 5.62/4.21 and 5.66/4.37 eV/nm, respectively (see Table S2 of ESI†). These formation energies are about 10% higher than those on pure Ni, Co surfaces, implies that the minor effect of the C solubility inside the catalyst on the graphene edge formation. Consequently, the H_2 pressure for the phase transition of graphene edges from the H-G to the M-G was slightly changed for both AC and ZZ edges but their order of stability remains (see ESI, Fig. S8†). Hence, we can conclude that the C solubility is a secondary factor for the edge phase diagram and growth kinetics of graphene on Ni and Co substrates.

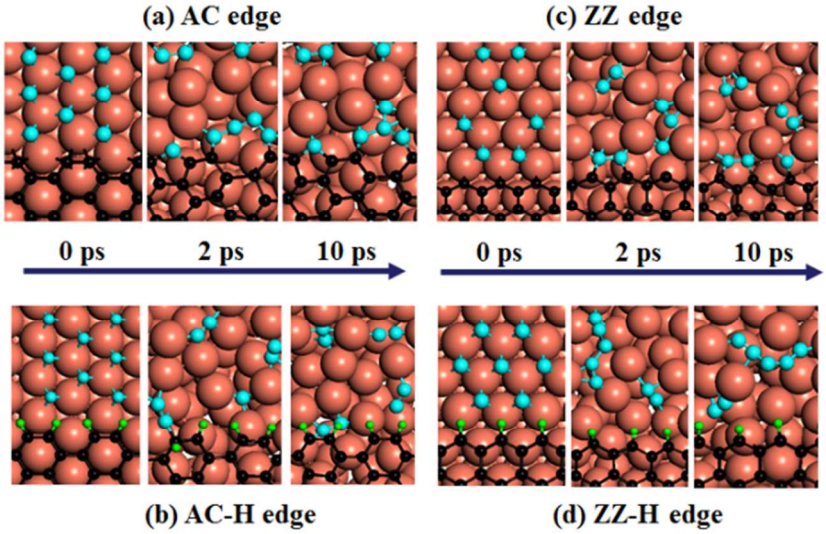

Fig. 3 Snapshots during the trajectories of *ab initio* MD simulations of the growth of (a) Cu-passivated zigzag (ZZ), (b) H-passivated ZZ (H-ZZ), (c) Cu-passivated armchair (AC), and (d) H-passivating AC (H-AC) graphene edges at 1500 K. The small green, medium black and large cyan balls on Cu(111) substrate represent the H atoms, the C atoms belongs to the graphene, and those dispersed C atoms on the Cu(111) surface , respectively..

Chemical Science

RSCPublishing

EDGE ARTICLE

The carbon addition from the metal surface to the edge of graphene dominates the kinetics of graphene CVD growth. According to the theory of kinetic Wulff construction (KWC) (see ESI, Fig. S9†), the edge that grows slowest dominates the circumference of a graphene domain[10, 42, 45, 46]. For a H-**G** edge, as all the dangling bonds are saturated, the addition of more C atoms to the edge requires to break the strong C-H bond and thus is normally very difficult to be achieved. In contrast, for a **M-G** edge, each edge atom of graphene contacts with a few metal atoms and thus the addition of C atoms from the metal surface to the graphene edge should be much easier. Such a difference can be clearly seen in the MD simulation shown in Fig. 3**.** At 1500 K and in 10 ps, the dispersed C atoms easily attach to the edge of both AC and ZZ M-G graphene edges Cu(111) surface (Fig. 3a and Fig. 3c) . Although there's no enough time to heal the defects formed during the C addition, the relatively high activity of the **M-G** edge is clearly demonstrated. In sharp contrast, there's no C atom attached to the **H-G** edge in another simulation performed under exact same condition, which clearly presenting the inertness of the **H-G** edge (Fig. 3b and Fig. 3d).

To fully understand the evolution of graphene domain in the CVD growth, the knowledge of the growth rate of various types of graphene edges, such as AC, ZZ and those titled ones in between, is required. In previous studies, it is well established that, a kink site (either AC kink or ZZ kink) of a **M-G** edge acts as an active site for the sinking of new C atoms and thus the edge with more kinks grows faster[42,46-49]. For the two edges without any kinks, the ZZ edge grows slower than the AC edge because of its large kink height[42]**.** From this analysis, we can simply draw a conclusion that the ZZ edges should be the one grows slowest. As a consequence of the KWC, the regular graphene domain with M-G edges should have a hexagonal shape with zigzag edges, which is in agreement with many experimental observations[19-30].

In the range of high H_2 pressure on metal surfaces, both AC and ZZ edges are hydrogen terminated. During growth, incorporating C atoms to the H-terminated edges are very difficult due to the inertness of the H-G edge. As an example, the atomic structures and threshold barriers for the incorporation of C atoms at the H terminated AC and ZZ edges on Cu(111) surface are shown in Fig. 4(a) and Fig. 4(b), respectively (see ESI† for the computational details). For the H-terminated AC edge, a repeatable cycle of graphene growth requires the addition of two C atoms in sequence to produce a new hexagon at an AC site. Fig. 4a shows the lowest-energy path of forming a new hexagon at the AC edge. It can be found that the incorporation of the second C atom is the threshold step with the threshold energy of 4.55 eV. For the ZZ edge, to form the first hexagon on the continuous edge requires the addition of three C atoms and the threshold step appears during the addition of the second C atom with the threshold energy of 4.68 eV (Fig. 4b), which is just a bit higher than that of the AC edge growth. Although the threshold energies are very similar for the growth of both AC and ZZ edges, the requirement of three atoms to form a hexagonal ring at the ZZ edge implies that the growth rate of ZZ edge $R_{ZZ} \sim [(c - c_{eq})/c_{eq}]^3$, which must be much slower than that of AC edge $R_{AC} \sim [(c - c_{eq})/c_{eq}]^2$ because the supersaturation level of active carbon, $(c - c_{eq})/c_{eq}$, normally far less than 1, where c and c_{eq} are the concentration of C atoms during growth and under equilibrium, respectively. $R_{AC} > R_{ZZ}$ implies that H-terminated graphene edges also prefer the ZZ type during growth and the shape of a growing graphene domain should be a hexagon as well (Fig. 5).

Above analysis indicates that both metal-passivated and H-terminated graphene domains tend to have a hexagonal shape with six ZZ edges in the parameter region of (*i*) — high T and low p (Fig. 5) and (*ii*) — low T and high p (Fig. 5). Now let's turn to the region (*iii*) in the diagram, where the AC edge is terminated by H and the ZZ edge is passivated by the catalyst surface. For graphene growth on Cu(111) surface at a typical CVD temperature (~ 1300K), the H_2 partial pressure ranges from 10^{-2} to 10^{-5} Torr. Because the metal-supported ZZ edge grows faster than H-passivated AC edge (Figure 3), a growing graphene domain should be dominated by the edge type that grows slowest, which is the H terminated AC edge. As a consequence, the growing graphene domains in this region should have a hexagonal shape with six H terminated AC edges (Fig. 5).

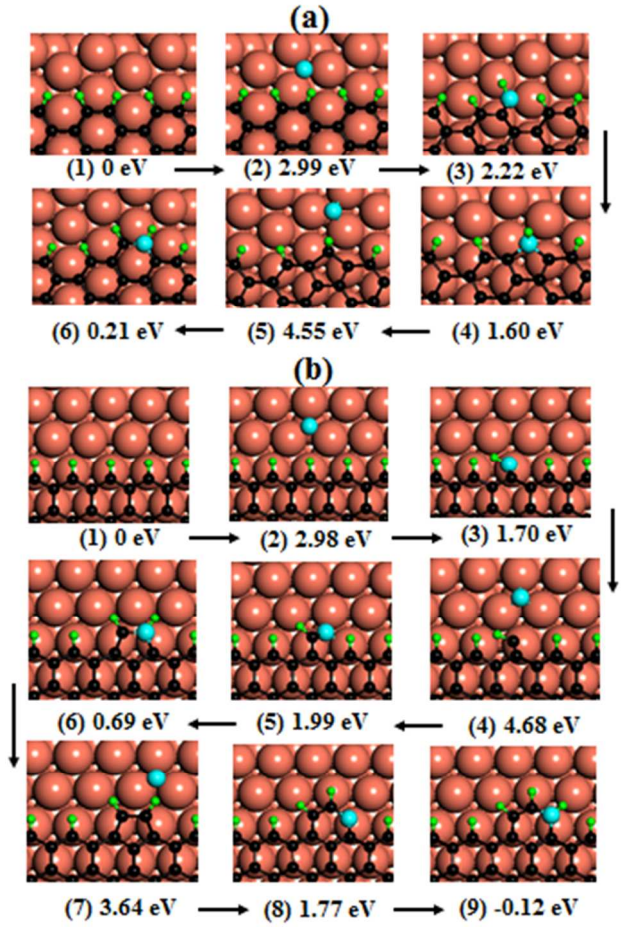

Fig. 4 The incorporation of C atoms at the H-passivated (a) armchair and (b) zigzag graphene edges on Cu(111) surface to form a new hexagon, respectively. The green, black balls represent H, C atoms in graphene and the blue and orange balls represent the attached C atoms and the Cu atoms, respectively. The formation energies calculated by using the energy of H_2 molecule as reference in eV are shown under each panel.

On the other side, an active M-G edge tends to quickly adsorb all carbon atoms that approach to it. However, the growth rate would highly depend on the diffusion of active carbon species on the catalyst surface if the carbon supply is not sufficient. Among the known catalyst for graphene growth, Cu and Au are two less active ones and the barrier of decomposing feedstock, such as CH_4, on them was proved high and thus the carbon supply for graphene growth may be not sufficient[7]. Hence, it is possible to observe the diffusion limited growth (DLG) behaviour and fractal like graphene domains on Cu and Au surfaces at the region (*i*)—where temperature *T* is high and H_2 partial pressure *p* is low (Fig. 5). On other transition metals which are more active, such as Ni, Co, Fe Pt, Pd, Ru, Rh, Ir,[8-10] the observation of the DLG would be very difficult because of the high rates of feedstock decomposition on these metal surfaces.

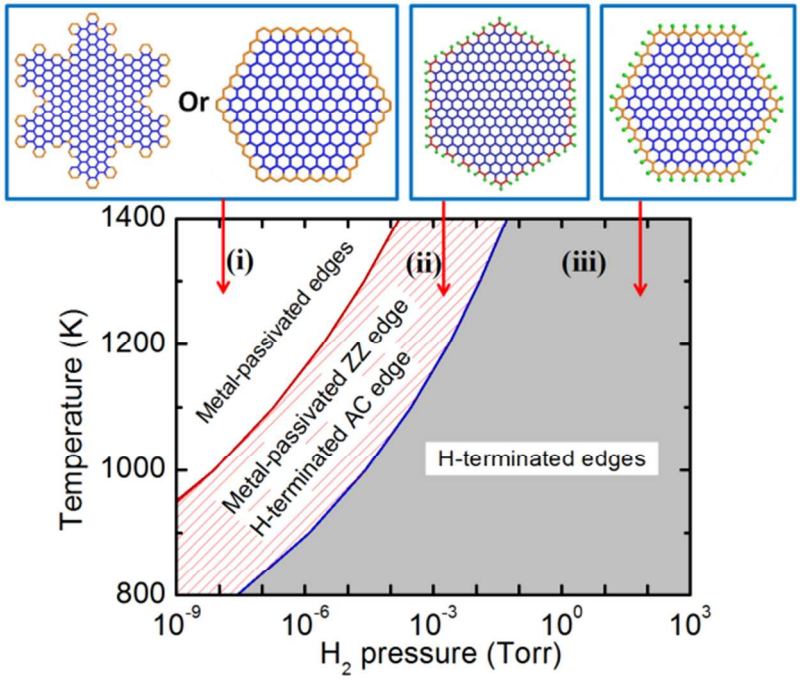

Fig. 5 The diagram of graphene AC and ZZ edges on Cu(111) surface and the corresponding possible shapes of graphene domains grown in each region—metal passivated fractal-like domains or regular ZZ edged hexagons in (**i**), H terminated AC edged hexagon domains in (**ii**) and hydrogen terminated ZZ edged hexagon domain in (**iii**).

Conclusions

In summary, our theoretical investigation on the diagram and growth kinetics of graphene edges in chemical vapor deposition (CVD) growth on four typical metal surfaces (Au(111), Cu(111), Ni(111), and Co(0001)) demonstrates that temperature, *T*, and H_2 partial pressure *p*, dependent growth behavior includes three parameter regions. At high *T* and low *p*, both AC and ZZ edges are metal passivated and grow fast. At high *p* and low *T*, both AC and ZZ graphene edges are H terminated and grow slow. Beyond, the steady state shape of graphene domain in CVD growth are predicated to be ZZ edged hexagons for both cases, which is in good agreement with broadly observed experiments. Within an appropriate *p* and *T* range (e.g. 10^{-2}~ 10^{-5} Torr and 1300 K on Cu(111)), an unexpected formation of graphene domain—hexagonal shape with six AC edges is predicated because the H termination occurs on the AC edge only. Our result provides a theoretical guidance for controlling the edge structure and morphology of graphene in the CVD growth.

Acknowledgements

This work was supported in part by Hong Kong RGC-GRF grants (B-Q35N and B-Q26K), NSFC grant (21273189 and 11404309). Computational resources from the Shanghai and Tianjin Supercomputer Centers are acknowledged.

Notes and references

[a] *National Laboratory for Infrared Physics, Shanghai Institute of Technical Physics, Chinese Academy of Science, 200083 Shanghai, China; ; E-mail: Feng.Ding@polyu.edu.hk*
[b] *Institute of Textiles and Clothing, Hong Kong Polytechnic University, Hong Kong, China*

† Electronic Supplementary Information (ESI) available: Atomic structures of freestanding, metal-passivated, and H-terminated graphene nanoribbons; Energy convergence of graphene nanoribbons on Cu(111) surface with respect to the k-point mesh and the thickness of vacuum layer; The computational models for calculating formation energies of graphene edges on metal surfaces; The computational details for thermodynamic phase diagrams of graphene edges; Computational details for formation energies and phase diagrams of graphene edges on Ni and Co substrates with surface carbide; The experimental parameters and the corresponding growing graphene morphology; Kinetic Wulff construction; Computational details of threshold energies for the incorporation of C atoms at H-passivated graphene edges. See DOI: 10.1039/b000000x/

1 K. S. Novoselov, A. K. Geim, S. V. Morozov, D. Jiang, Y. Zhang, S. V. Dubonos, I. V. Grigorieva and A. A. Firsov, *Science*, 2012, **306**, 666-669.
2 H. Chen, W. G. Zhu and Z. Y. Zhang, *Phys. Rev. Lett.*, 2010, **104**, 186101.
3 W. Chen, H. Chen, H. P. Lan, P. Cui, T. P. Schulze, W. G. Zhu and Z. Y. Zhang, *Phys. Rev. Lett.*, 2012, **109**, 265507.
4 D. J. Cheng, G. Barcaro, J. C. Charlier, M. Hou and A. Fortunelli, *J. Phys. Chem. C*, 2011, **115**, 10537-10543.
5 Y. Wang, A. J. Page, Y. Nishimoto, H. J. Qian, K. Morokuma and S. Irle, *J. Am. Chem. Soc.*, 2011, **133**, 18837-18842.
6 P. Wu, H. J. Jiang, W. H. Zhang, Z. Y. Li, Z. H. Hou and J. L. Yang, *J. Am. Chem. Soc.*, 2012, **134**, 6045-6051.
7 W. H. Zhang, P. Wu, Z. Y. Li and J. L. Yang, *J. Phys. Chem. C*, 2011, **115**, 17782-17787.
8 J. F. Gao, J. Yip, J. J. Zhao, B. I. Yakobson and F. Ding, *J. Am. Chem. Soc.*, 2011, **133**, 5009-5015.
9 Q. H. Yuan, J. F. Gao, H. B. Shu, J. J. Zhao, X. S. Chen and F. Ding, *J. Am. Chem. Soc.*, 2012, **134**, 2970-2975.
10 H. B. Shu, X. S. Chen, X. M. Tao and F. Ding, *ACS Nano*, 2012, 6, 3243-3250.
11 J. A. Elliott, Y. Shibuta, H. Amara, C. Bichara and E. C. Neyts, *Nanoscale*, 2013, **5**, 6662
12 Y. Wang, A. J. Page, H. B. Li, H. J. Qian, M. G. Jiao, Z. J. Wu, K. Morokuma and S. Irle, *Nanoscale*, 2014, **6**, 140.
13 L. Meng, Q. Sun, J. Wang and F. Ding, *J. Phys. Chem. C*, 2012, **116**, 6097.
14 Y. Shibuta, R. Arifin, K. Shimamura, T. Oguri, F. Shimojo and S. Yamaguchi, *Chem. Phys. Lett.*, 2013, **565**, 92.
15 T. Paronyan, E. M. Pigos, G. Chen and A. R. Harutyunyan, *ACS Nano*, 2011, **5**, 9619-9627.
16 X. S. Li, C. W. Magnuson, A.Venugopal, R. M. Tromp, J. B. Hannon, E. M. Vogel, L. Colombo and R. S. Ruoff, *J. Am. Chem. Soc.*, 2011, **133**, 2816-2819.
17 Y. Zhang, L. Y. Zhang, P. Kim, M. Y. Ge, Z. Li and C. W. Zhou, *Nano Lett.*, 2012, **12**, 2810-2816.
18 D. Geng, B. Wu, Y. Guo, L. Huang, Y. Xue, J. Chen, G. Yu, L. Jiang, W. Hu and Y. Liu, *Proc. Nat. Acad. Sci. U. S. A.*, 2012, **109**, 7992-7996.
19 X. F. Zhang, J. Ning, X. L. Li, B. Wang, L. Hao, M. H. Liang, M. H. Lin and L. J. Zhi, *Nanoscale*, 2013, **5,** 8363.
20 W. Wu, L. A. Jauregui, Z. Su, Z. Liu, J. Bao, Y. P. Chen and Q. Yu, *Adv. Mater.*, 2011, **23**, 4898-4903.
21 P. Egberts, G. H. Han, X. Z. Liu, A. T. C. Johnson and R. W. Carpick, *ACS Nano*, 2014, **8**, 5010-5012.
22 B. Wu, D. C. Geng, Y. L. Guo, L. P. Huang, Y. Z. Xue, J. Zheng, J. Chen, G. Yu, Y. Q. Liu, L. Jiang and W. P. Hu, *Adv. Mater.*, 2011, **23**, 3522-3525.
23 Y. Zheng, J. Lin, Z. W. Peng, Z. Z. Sun, Y. Zhu, L. Li, C. S. Xiang, E. L. Samuel, C. Kitrell and J. M. Tour, *ACS Nano*, 2012, **6**, 9110-9117.
24 A. Mohsin, L. Liu, P. Z. Liu, W. Deng, I. N. Ivanov, G. Li, O. E. Dyck, G. Duscher, J. R. Dunlap, K. Xiao and G. Gu, ACS Nano, 2013, **7**, 8924-8931.
25 B. Wang, X. F. Ma, M. Caffio, R. Schaub and W. X. Li, *Nano Lett.*, 2011, **11**, 424-430.
26 D. Prezzi, D. Eom, K. T. Rim, H. Zhou, S. X. Xiao, C. Nuckolls, T. F. Heinz, G. W. Flynn and M. S. Hybertsen, *ACS Nano*, 2014, **8**, 5765-5773.
27 N. Liu, L. Fu, B. Dai, K. Yan, X. Liu, R. Q. Zhao, Y. F. Zhang and Z. F. Liu, *Nano Lett.*, 2011, **11**, 297-303.
28 L. Gao, W. C. Ren, H. L. Xu, L. Jin, Z. X. Wang, T. Ma, L. P. Ma, Z. Y. Zhang, Q. Fu, L. M. Peng, X. H. Bao and H. M. Cheng, *Nat. Comm.*, 2011, 3, 699.
29 B. Y. Pan, H. G. Zhang, D. X. Shi, J. T. Sun, S. X. Du, F. Liu and H. J. Gao, *Adv. Mater.*, 2009, **21**, 2777-2780.
30 Z. Yan, Z. W. Peng and J. M. Tour, *Acc. Chem. Res.*, 2014, **47**, 1327-1337.
31 D. N. Petsev, K. Chen, O. Gliko and P. G. Vekilov, *Proc. Nat. Acad. Sci. U. S. A.*, 2002, **100**, 792-796.
32 E. Ringe, R. P. Van Duyne and L. D. Marks, *J. Phys. Chem. C*, 2013, **117**, 15859-15870.
33 P. E. Blöchl, *Phys. Rev. B*, 1994, **50**, 17953-17979.
34 G. Kresse and J. Furthmüller, *Phys. Rev. B*, 1996, **54**, 11169-11186.
35 J. P. Perdew, K. Burke and M. Ernzerhof, *Phys. Rev. Lett.*, 1996, 77, 3865-3868.
36 G. Kresse and D. Joubert, *Phys. Rev. B*, 1999, **59**, 1758-1775.
37 D. Li, P. Zhang and J. Yan, *Sci. Rep.*, 2014, **4**, 4707.
38 S. Günther, S. Dänhardt, B. Wang, M. L. Bocquet, S. Schmitt and J. Wintterlin, *Nano Lett.*, 2011, **11**, 1895-1900.
39 X. Y. Zhang, L. Wang, J. Xin, B. I. Yakobson and F. Ding, *J. Am. Chem. Soc.*, 2014, **136**, 3040-3047
40 I. Vlassiouk, M. Regmi, P. Fulvio, S. Dai, P. Datskos, G. Eres and S. Smirnov, *ACS Nano*, 2011, 5, 6069-6076.
41 A. T. Murdock, A. Koos, T. B. Britton, L. Houben, T. Batten, T. Zhang, A. J. Wilkinson, R. E. Dunin-Borkowski, C. E. Lekka and N. Grobert, *ACS Nano*, 2013, 7, 1351-1359.
42 T. Ma, W. C. Ren, X. Y. Zhang, Z. B. Liu, Y. Gao, L. C. Yin, X. L. Ma, F. Ding and H. M. Cheng, *Proc. Nat. Acad. Sci. U. S. A.*, 2013, **110**, 20386-20391.
43 X. Li, W. Cai, L. Colombo and R. S. Ruoff, *Nano Lett.*, 2009, **9**, 4268-4272.
44 J. Lahiri, T. Miller, L. Adamska, I. I. Oleynik and M. Batzill, *Nano Lett.*, 2011, **11**, 518-522
45 L. Wang, X. Y. Zhang, H. L. W. Chan, F. Yan and F. Ding, *J. Am. Chem. Soc.*, 2013, **135**, 4476-4482.
46 V. I. Artyukhov, Y. Y. Liu and B. I. Yakobson, *Proc. Nat. Acad. Sci. U. S. A.*, 2012, **109**, 15136-15140.
47 F. Ding, A. R. Harutyunyan and B. I. Yakobson, *Proc. Nat. Acad. Sci. U. S. A.*, 2009, **106**, 2506-2509.
48 R. Rao, D. Liptak, T. Cherukuri, B. I. Yakobson and B. Maruyama, *Nat. Mater.*, 2012, **11**, 213-216.
49 Y. Liu, A. Dobrinsky and B. I. Yakobson, *Phys. Rev. Lett.*, 2010, **105**, 235502.